CHORS ∧∧∧ Center for Hydro-Optics & Remote Sensing

San Diego State University   6505 Alvarado Road, Suite 206   San Diego, CA 92120-5005   619/594-2272 or 594-2230

CHORS Technical Memorandum 007-93

INVESTIGATION OF OCEAN BIO–OPTICAL VARIABILITY USING THE MULTISPECTRAL AIRBORNE RADIOMETER SYSTEM (MARS)
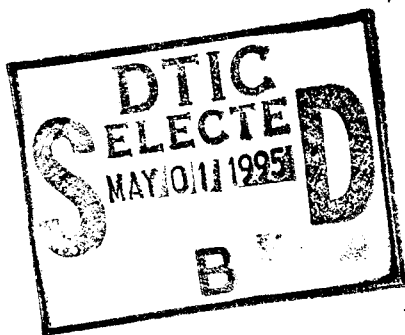
7 July 1993

by

James L. Mueller

Incorporating contributions by
Dr. R. Edward Lange
(Deceased, 14 April 1990)

San Diego State University
Center for Hydro-Optics and Remote Sensing
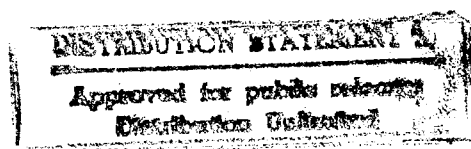6505 Alvarado Road, Suite 206
San Diego, CA 92120

Final Technical Report

ONR Grant N00014-89-J-1468

19950428 081

REPORT DOCUMENTATION PAGE

Form Approved
OMB No. 0704-0188

Public reporting burden for this collection of information is estimated to average 1 hour per response, including the time for reviewing instructions, searching existing data sources, gathering and maintaining the data needed, and completing and reviewing the collection of information. Send comments regarding this burden estimate or any other aspect of this collection of information, including suggestions for reducing this burden, to Washington Headquarters Services, Directorate for Information Operations and Reports, 1215 Jefferson Davis Highway, Suite 1204, Arlington, VA 22202-4302, and to the Office of Management and Budget, Paperwork Reduction Project (0704-0188), Washington, DC 20503.

1. AGENCY USE ONLY (Leave blank)	2. REPORT DATE 7 JULY 1993	3. REPORT TYPE AND DATES COVERED FINAL TECHNICAL REPORT

4. TITLE AND SUBTITLE	5. FUNDING NUMBERS
INVESTIGATION OF OCEAN BIO-OPTICAL VARIABILITY USING THE MULTISPECTRAL AIRBORNE RADIOMETER SYSTEM (MARS)	
6. AUTHOR(S) JAMES L. MUELLER, WITH R.E. LANGE (DECEASED)	N00014-89J-1468

7. PERFORMING ORGANIZATION NAME(S) AND ADDRESS(ES)	8. PERFORMING ORGANIZATION REPORT NUMBER
CENTER FOR HYDRO-OPTICS AND REMOTE SENSING SAN DIEGO STATE UNIVERSITY 6505 ALVARADO RD., SUITE 206 SAN DIEGO, CA 92120-5005	CHORS TM 007-93

9. SPONSORING / MONITORING AGENCY NAME(S) AND ADDRESS(ES)	10. SPONSORING / MONITORING AGENCY REPORT NUMBER
DR. RICHARD SPINRAD OCEAN SCIENCES, CODE 1173 OFFICE OF NAVAL RESEARCH 800 N. QUINCY STREET ARLINGTON, VA 22217-5000	—

11. SUPPLEMENTARY NOTES

NONE

12a. DISTRIBUTION / AVAILABILITY STATEMENT	12b. DISTRIBUTION CODE
UNLIMITED DISTRIBUTION	—

13. ABSTRACT (Maximum 200 words)

AN EXISTING MULTISPECTRAL AIRBORNE RADIOMETER SYSTEM (MARS) WAS UP-GRADED TO INCLUDE MEASUREMENT OF DOWNWELLING SPECTRAL IRRADIANCE, AS WELL AS UPWELLED SPECTRAL RADIANCE, FROM AIRCRAFT OF OPPORTUNITY. THE MARS WAS DEPLOYED OVER THE NORTH ATLANTIC OCEAN ABOARD NASA'S P-3 AIRCRAFT DURING THE JGOFS NORTH ATLANTIC BLOOM EXPERIMENT IN 1989. ATMOSPHERIC AND SURFACE REFLECTION CORRECTIONS, AND OCEAN COLOR ALGORITHMS WERE APPLIED TO THE MARS DATA TO DERIVE TRANSECTS OF CHLOROPHYLL A CONCENTRATION ALONG AIRCRAFT TRACKLINES. RESULTS ARE GIVEN ALONG SELECTED FLIGHTLINES.

14. SUBJECT TERMS			15. NUMBER OF PAGES 34
OCEAN COLOR, AIRBORNE RADIOMETRY, OCEAN BIO-OPTICAL PROERTIES, N. ATLANTIC OCEAN, CHLOROPHYLL			16. PRICE CODE —

17. SECURITY CLASSIFICATION OF REPORT	18. SECURITY CLASSIFICATION OF THIS PAGE	19. SECURITY CLASSIFICATION OF ABSTRACT	20. LIMITATION OF ABSTRACT
UNCLASSIFIED	UNCLASSIFIED	UNCLASSIFIED	UL

NSN 7540-01-280-5500

Standard Form 298 (Rev. 2-89)
Prescribed by ANSI Std. Z39-18
298-102

TABLE OF CONTENTS

1.0 INTRODUCTION

The Multispectral Airborne Radiometer System (MARS) is a self–contained, lightweight, remote sensing system developed originally at the Visibility Laboratory (VISLAB), which was formerly a component of Scripps Institution of Oceanography. The MARS was enhanced by subsequent engineering modifications (under this grant) at the San Diego State University (SDSU) Center for Hydro–Optics and Remote Sensing (CHORS). Two engineering improvements to MARS were technical objectives of this grant. The principal scientific objective of the grant, however, was to apply the system to study bio–optical variability in the vicinity of the ONR Marine Light–Mixed Layer (MLML) mooring deployed near 60°N, 20°W in 1989, and along 20°W during the JGOFS North Atlantic Bloom Experiment (NABE).

The first MARS engineering upgrade, which was completed during year one of the grant period, was to add the capability to measure downwelling incident irradiance $E_d(\lambda)$ at 4 wavelengths. $E_d(\lambda)$ measurements are needed to accurately estimate normalized water–leaving radiance ratios $L_{wN}(\lambda_1)/L_{wN}(\lambda_2)$ from radiances $L(\lambda_1)$ and $L(\lambda_2)$ measured with the MARS at flight altitude.

The second engineering upgrade was a fundamental design modification to replace the 5–inch diameter, Barium–Sulfate coated (96% reflective) integrating sphere, with which MARS was originally configured, with a 3–inch diameter integrating sphere machined from Spectralon™ (99% reflectance). For the same field–of–view (fov), collection optics and scene radiance, the smaller, more reflective sphere delivers significantly more radiant flux to the filtered detectors, with a corresponding increase in the signal–to–noise ratio (SNR). This system modification was only partly completed (Sect. 2.2 below), because of the death of my Co–Principal Investigator, Dr. Ed Lange, near the end of the grant period. Fatal disruption of this phase of the work was one of several adverse impacts which stemmed directly from Dr. Lange's death and affected our overall performance under this grant.

The scientific objective of this grant was to utilize the MARS to measure spatial variability in bio–optical properties: a) near the site of the instrumented mooring deployed in 1989 at 65°N, 20°W for the ONR MLML program, and b) along 20°W longitude, between 45° and 65°N, during the JGOFS North Atlantic Bloom Experiment (NABE). Dr. Lange successfully acquired MARS data at these sites during the May/June 1989 mission of the P–3 remote sensing aircraft operated by NASA out of Wallops Flight Center (WFC), Wallops Island, VA. Dr. Lange had calibrated and nearly completed the analyses of these MARS data, and was preparing draft material for journal articles, in collaboration with me and colleagues at WFC and NOARL (now NRL Detachment, Stennis Space Center, MS), at the time of his death in the spring of 1990. Unfortunately, I have been able to reconstruct Dr. Lange's analyses only partially, and I am now in the process of reconstructing the data calibration and analyses

---

TM "Spectralon" is a registered trademark of Labview, Inc.
    P.O. Box 70
    North Sutton, NH 03260

of selected flight segments from the original MARS data files. This rework of the data is necessary to derive products of quality and traceability acceptable as a basis for journal publication.

In this Final Technical Report, I describe the engineering improvements made to MARS and the system's current engineering status. I also report the results from Dr. Lange's preliminary analyses of the MARS JGOFS (NABE)/MLML measurements over the North Atlantic Ocean in 1989, and describe recent work in progress on a manuscript to report the scientific results of the 1989 JGOFS (NABE)/MLML MARS measurements in collaboration with Dr. Charles Trees (CHORS; *in situ* bio–optical profile measurements aboard the Atlantis II), Dr. Frank Hoge [NASA WFC; Airborne Oceanographic LIDAR (AOL) measurements], and Mr. Robert Arnone [NRL Detachment, Stennis Space Center, MS; AXBT profiles and sea surface temperature traces across ocean fronts near Iceland].

2.0   METHODS AND ALGORITHMS FOR LOW ALTITUDE (NON–IMAGING) AIRBORNE OCEAN COLOR REMOTE SENSING

Airborne systems for remote sensing of ocean color may be based either on imaging spectral radiometers, or on radiometers which measure spectral radiance $L(\lambda)$ at a single, fixed set of nadir and azimuth viewing angles relative to the aircraft's heading. In this report we address only airborne remote sensing systems which measure spectral radiance in a single geometric fov, and thus measure a multispectral, 1–dimensional $L(\lambda)$ profile along an aircraft's trackline over the ocean's surface. These systems are suitable for measuring horizontal profiles of near–surface bio–optical properties [*e.g.* chlorophyll concentration and K(490)] over trackline distances totaling several hundred Km within the span of a few hours. This approach permits near–synoptic mapping of grid patterns to resolve oceanographic features with spatial scales ranging from a few Km to a few hundred Km (*i.e.* oceanic sub–mesoscale to mesoscale). These systems are not well suited for bio–optical mapping of either large scale ocean features (100 to 1000 Km scales: the proper domain for satellite ocean color images), or small–scale ocean or estuarine features (≤ 3 Km: the proper domain for airborne high–resolution ocean color imaging systems). In applications to intermediate scales, however, the single fov systems offer a cost–effective approach, with the added advantage of being able to operate under overcast conditions which preclude measurements from high–altitude aircraft, or spacecraft.

In order to accurately relate remotely sensed ocean color spectral radiance measurements $L(\lambda)$ to bio–optical variables, such as chlorophyll concentration C and diffuse attenuation coefficient K(490) (*e.g.* at a wavelength of 490 nm), it is necessary to first estimate values of water–leaving radiance $L_w(\lambda)$ backscattered from the upper water column and transmitted through the air–sea interface. Water–leaving radiance $L_w(\lambda)$ is related to radiance $L(\lambda)$ measured at altitude h as

$$L_w(\lambda) = t^{-1}(\lambda, h, \mu) \ L(\lambda) - L_{rs}(\lambda) - L_g(\lambda), \tag{1}$$

2

where $t(\lambda,h,\mu)$ is transmittance of the atmosphere from the surface pixel to the radiometer, μ is the cosine of the viewing zenith angle at the pixel (identical to the radiometer's nadir angle in this case), and $L_{rs}(\lambda)$ and $L_g(\lambda)$ are, respectively, skylight and direct sunlight reflected into the fov at the sea surface.

Although some airborne ocean color radiometers have been operated in a nadir viewing configuration (*e.g.* Hoge and Swift 1993), experience has shown that the nadir fov is almost always contaminated by sun glint (except under conditions of complete overcast). It is generally prudent, therefore, to orient the fov at an azimuth which points away from the sun, and which also avoids viewing the aircraft's shadow on the sea surface (*e.g.* Mueller 1976, and Mueller and Trees 1989).

In use, single fov ocean color radiometers are typically operated at flight altitudes of only ~300 m above the sea surface. Accurate corrections for atmosphere attenuation and path radiance are, therefore, far less critical than is the case for ocean color measurements from high altitude or space, where radiance just above the sea surface may comprise only 10% to 20% of the measured aperture radiance (Gordon *et al.* 1983). However, reflections of incident sky radiance at the sea surface are equally present in both types of measurement, and in general, may be more difficult to remove from low altitude radiance measurements. By definition, the spacecraft always views the ocean under clear-sky conditions, and as a result the surface reflection components can be absorbed into the atmospheric Raleigh scattering correction with acceptable accuracy and relative ease. On the other hand, a low altitude airborne ocean color system must often be operated under a variety of cloud conditions, which may significantly alter the intensity and spectral quality of incident irradiance, and thus directly affect the spectra of both water-leaving radiance $L_w(\lambda)$ and surface reflected skylight $L_{rs}(\lambda)$. (Of course if sun glint $L_g(\lambda)$ is present in the fov, then the surface reflection component becomes a much larger fraction of the total signal, and accurate corrections will become correspondingly more difficult to achieve.)

Assuming that we direct the fov to avoid sun glint, we may assume $L_g(\lambda) \equiv 0$ and reduce Eq. (1) to

$$L_w(\lambda) = t^{-1}(\lambda,h,\mu)\ L(\lambda) - L_{rs}(\lambda). \tag{2}$$

We may write reflected skylight as

$$L_{rs}(\lambda) = \rho(\lambda,\mu)\ L_s(\lambda,\mu,\phi), \tag{3}$$

where $L_s(\lambda)$ is "effective" sky radiance at wavelength λ and the viewing zenith cosine μ and azimuth angle ϕ, and $\rho(\lambda,\mu)$ is the effective reflectance of the sea surface at wavelength λ and zenith cosine μ. Were the sea surface flat, then $\rho(\lambda,\mu)$ would equal the Fresnel reflectance, and $L_s(\lambda,\mu,\phi)$ would be sky radiance incident at the pixel in a solid angle equal to the radiometer's fov. In practice however, the

sea surface is always roughened by waves and $L_{rs}(\lambda)$ actually depends on the of the product of sky radiance distribution, Fresnel reflectance, and the slope distribution of the wind–roughened sea surface (Cox and Munk 1956) integrated over a solid angle subtense of the sky which is significantly larger than the fov.

We will attempt to circumvent this difficult problem by assuming first that $L_w(\lambda_r) \equiv 0$ at a near–infrared wavelength λ_r, so that combining (2) and (3) we obtain

$$\rho(\lambda_r, \mu)\, L_s(\lambda_r, \mu, \phi) = \tau^{-1}(\lambda_r, \mu)\ L(\lambda_r). \tag{4}$$

The wavelength dependence of $\rho(\lambda, \mu)$ is the same that of Fresnel reflectance, which is small, so that we may neglect it, *i.e.* we assume

$$\rho(\lambda, \mu) = \rho, \tag{5}$$

a constant for all wavelengths at a fixed viewing zenith cosine. We may thus write for wavelengths λ and λ_r that

$$\frac{L_{rs}(\lambda)}{L_{rs}(\lambda_r)} = \frac{L_s(\lambda, \mu, \phi)}{L_s(\lambda_r, \mu, \phi)} \tag{6}$$

and from (4) and (5)

$$L_{rs}(\lambda) = \left[\frac{L_s(\lambda, \mu, \phi)}{L_s(\lambda_r, \mu, \phi)} \right] \bullet t^{-1}(\lambda_r, \mu)\ L(\lambda_r). \tag{7}$$

We further assume that $t(\lambda_r, \mu) \cong 1$ over the short atmospheric path length being considered here, and that

$$\frac{L_s(\lambda, \mu, \phi)}{L_s(\lambda_r, \mu, \phi)} \cong \frac{E'_d(\lambda)}{E'_d(\lambda_r)}, \tag{8}$$

where $E'_d(\lambda)$ is the incident irradiance which would be measured were the entire sky covered with cloud conditions equivalent to those in the sky sector contributing to reflected skylight. Our problem then reduces to one of estimating the ratio

$$\varsigma(\lambda, \lambda_r) \equiv \frac{E'_d(\lambda)}{E'_d(\lambda_r)} \tag{9}$$

for each pixel.

The most widely known in–water algorithms for estimating phytoplankton pigment concentrations and diffuse attenuation coefficient K(490) were developed for use with data from the Nimbus–7 Coastal Zone Color Scanner (CZCS). The original CZCS algorithm for pigment concentrations C is (Gordon *et al.* 1983)

4

$$C_1 = 1.129 \left[\frac{L_w(443)}{L_w(550)} \right]^{-1.711}, \tag{10}$$

$$C_2 = 3.326 \left[\frac{L_w(520)}{L_w(550)} \right]^{-2.439} \tag{11}$$

with the selection rule that if $C_1 \leq 1.5$ mg m^{-3} then $C = C_1$, or else $C = C_2$. The CZCS algorithm for diffuse attenuation $K(490)$ is (Austin and Petzold 1981)

$$K(490) = 0.0220 + 0.0883 \left[\frac{L_w(443)}{L_w(550)} \right]^{-1.491}. \tag{12}$$

Equations (10) through (12) are all based on ratios of water–leaving radiances, as measured directly without adjustment for solar zenith distance, but under clear–sky conditions. More recent practice is to base algorithms on "normalized water–leaving radiances", $L_{wN}(\lambda)$ defined by Gordon (1990) to be water–leaving radiance which would have existed for a zenith sun and without an intervening atmosphere. Assuming that, for a given water column, radiance reflectance

$$R_L(\lambda) = \frac{\pi L_u(\lambda)}{E_d(\lambda)} \sim \text{constant}, \tag{13}$$

i.e. that it is negligibly dependent on the radiance distribution, we may calculate normalized water–leaving radiance as

$$L_{wN}(\lambda) = t_f(\lambda) \frac{R_L(\lambda)}{\pi} \bullet F(\lambda), \tag{14}$$

where $F(\lambda)$ is incident solar irradiance above the earth's atmosphere, and $t_f(\lambda)$ is Fresnel transmittance at the air–sea interface. We may rewrite (14) more explicitly in terms of directly measured (or estimated) water–leaving radiance $L_w(\lambda)$ and $E_d(\lambda)$ as

$$L_{wN}(\lambda) = L_w(\lambda) \frac{F(\lambda)}{E_d(\lambda)}. \tag{15}$$

It is then straightforward to combine (9) and (15) to express ratios of normalized water–leaving radiance as

$$\frac{L_{wN}(\lambda_1)}{L_{wN}(\lambda_2)} = \frac{L_w(\lambda_1)}{L_w(\lambda_2)} \bullet \frac{\varsigma(\lambda_2,\lambda_r)}{\varsigma(\lambda_1,\lambda_r)} \bullet \frac{F(\lambda_1)}{F(\lambda_2)}. \tag{16}$$

In (14) through (16), $F(\lambda)$ values are usually taken from Neckel and Labs (1984).

Finally, we may substitute Eqs. (2), (7), (8) and (9) into (16) to obtain

$$\frac{L_{wN}(\lambda_1)}{L_{wN}(\lambda_2)} = \frac{\left[t^{-1}(\lambda_1,\mu) \, L(\lambda_1) - \varsigma(\lambda_1,\lambda_r) \, L(\lambda_r) \right] \varsigma(\lambda_2,\lambda_r) F(\lambda_1)}{\left[t^{-1}(\lambda_2,\mu) \, L(\lambda_2) - \varsigma(\lambda_2,\lambda_r) \, L(\lambda_r) \right] \varsigma(\lambda_1,\lambda_r) F(\lambda_2)}, \tag{17}$$

Equation (17) represents one model (based on the chain of assumptions described above) for estimating normalized water–leaving radiance ratios using radiance measurements from low–altitude aircraft. These ratios may then be substituted into algorithms similar to Eqs. (10) through (12) to calculate chlorophyll concentration C and K(490).

The crucial factor governing the accuracy with which Eq. (17) may be applied to airborne ocean color data (assuming accurate radiometry), is the accuracy with which irradiance ratios $\varsigma(\lambda,\lambda_r)$ may be determined.

The simplest multispectral airborne radiometer systems include no capability for measuring downwelling irradiance $E_d(\lambda)$. Users of these systems must resort to *ad hoc* nominal approximations to $\varsigma(\lambda,\lambda_r)$ [Eq. (9)], which at best, may be based on regional, but non–concurrent, measurements of $E_d(\lambda)$ (*e.g.* from research vessels or at shore stations) (Mueller, 1974, 1976; Mueller and Trees 1989).

Significant improvements accrue if $E_d(\lambda)$ is measured concurrently with $L(\lambda)$, preferably at every wavelength of interest, but as a minimum, at enough wavelengths to allow interpolation of $\varsigma(\lambda,\lambda_r)$ to each (λ). Straightforward corrections to $L(\lambda)$, based on direct normalization with concurrently measured $E_d(\lambda)$ values, are simple to apply and yield obvious improvements (*e.g.* Fig. 4 in Sect. 4.3 below; Hoge and Swift 1993). However, the resulting $L_{wN}(\lambda)$ ratio estimates and derived bio-optical parameter estimates tend to be noisy when this technique is applied in the presence of locally variable cloud cover. This noise occurs primarily, because at any time t, the irradiance collector mounted on top of the aircraft is spatially removed (by ~80 m) from the pixel area on the sea surface which is viewed by the radiance channels, and because $E_d(\lambda)$ represents the entire sky dome, rather than the solid angle substense from which skylight is reflected.

Our proposed approach to obtaining improved estimates of $\varsigma(\lambda,\lambda_r,t)$ at time t is to determine, from measured $L(\lambda_r)$, $E_d(\lambda)$ and $E_d(\lambda_r)$ data in each time window $(t-\delta_t$ to $t+\delta_t)$, of duration between 15 and 120 seconds (to be determined in each case, depending on local cloud variability), by finding least–squares regression functions

$$\hat{\varsigma}(\lambda,\lambda_r t) = f \: [L(\lambda_r), \: t, \: \delta_t] \tag{18}$$

to characterize $\hat{\varsigma}(\lambda,\lambda_r,t)$ as a local function of $L(\lambda_r)$, for each wavelength λ, and at each position (indexed by time t) along a data trackline.

3.0 MARS ENGINEERING CONFIGURATION AND DEVELOPMENT

The MARS is designed to enable the collection of high quality ocean color data from aircraft of opportunity. It is a robust, portable, field instrument whose calibration is stable to within < 5% over the period of a typical deployment.

As the need developed for a small, easily deployable ocean color radiometer, the Visibility Laboratory, in conjunction with C.R. Booth of Biospherical Instruments Inc., undertook the development of a prototype instrument whose design included state of the art data acquisition technology, as well as high quality optical components. To achieve maximum radiometric accuracy in a small unit, it was necessary to design an optical collection system that was not dependent upon scene content variations within one field–of–view, that minimized the effects of path and surface reflection induced polarization, and that provided a common, spatially averaged field–of–view for 10 separate detectors at different wavelengths. These design criteria were realized by using a small integrating sphere as the radiance collector. After entering the sphere through the focusing and field limiting optics, light is defocused and effectively randomized through multiple reflections, before reaching the silicon diode detectors within the sphere. Furthermore, the flux is depolarized during the process of diffuse scattering within the sphere, and radiance fluctuations due to reflectance variations within the field–of–view are effectively smoothed and integrated into a common field–of–view for all 10 detectors.

The light detectors used in the MARS are ultraviolet enhanced silicon diodes mounted within TO–5 cans. Custom designed three cavity interference filters are used to spectrally divide the light into nominal 10 nm HPFW bands distributed throughout the visible and near–infrared part of the spectrum. The ten radiance detectors are situated near the equator of the sphere (Fig. 1). Each views a circular area on the opposite wall, which does not include the direct image projection, opposing silicon diode ports, or the entrance aperture of the sphere. With this alignment, light entering the sphere must undergo a minimum of two diffuse scatterings from the sphere's Barium–Sulfate wall before entering a detector port, and the average light ray undergoes many more reflections. Because this is a fixed, sealed system, responsivity drifts due to amplifier, reflective coating and diode changes with time, are minimized, and can be documented from a time history of laboratory calibrations.

Each of up to fourteen MARS channels is sampled by an analog to digital converter/variable amplifier gain loop under computer control; in addition to the 10 downlooking radiance $L(\lambda)$ channels, a separate irradiance unit was added to measure $E_d(\lambda)$ at 4 wavelengths (Sect. 3.2 below). Computer selectable gains are chosen to optimize signal/digitization noise for each individual sample. The internal computer can be programmed to average a selected number of measurements before transmitting the average to the data storage system. As configured for the MLML/JGOFS deployment, each of the system's fourteen channels was sampled 16 times, and an average value determined for each channel, prior to sending the data to the recording device. Data were acquired

every 0.008 seconds, and averaged data for all fourteen channels were transmitted to the storage device every 0.6 seconds, approximately. Because the time constant of each diode/amplifier circuit is on the order of 10 Hz, this sampling scheme provides for a better than 2 to 1 oversampling of the instrument response properties.

Temperature variations, electrical supply inconstancies, and vibration are relatively large in the aircraft environment. The MARS was designed to minimize the effect of these environmental factors. A shorted current loop amplifier with ultra low dc drift is used to amplify the diode signals, which are in the femto-ampere range. This mode of operation is found experimentally to be the least temperature sensitive mode for silicon diode detectors. The instrument is shock mounted with vibrationally loose coupling optimized for the small aircraft environment. The MARS has its own rechargeable battery pack, which also operates the data recording equipment (a lap-top computer) and provides up to 12 hours operation between charges. The instrument's power source and data collection computer are thus electrically isolated from the aircraft, except for a system ground to prevent static build-up on the instrument case, and the shielded coaxial signal and power cables. In this way the instrument is as electrically shielded as possible from stray static and radio frequency disturbances within the plane.

In appearance, the MARS is a box approximately 9 inches on a side. It has cable ports on the back side, along with an on/off switch. The front side mounts a standard Canon 50 mm F2 lens. The instrument mounts on two "u" shaped bracket rails (on the front surface), which are in turn attached to a circular azimuth mounting plate through four light duty rubber shock mounts. The circular azimuth mounting plate is designed to be held in place by four "pinch ties" that close on it like a disc brake. The base plate holding the "pinch tie" mountings is intended to be hard mounted on any aircraft camera port. The mounting should be installed loose enough to tolerate severe temperature changes and damp mechanical vibrations. During deployment, the instrument can be tilted at different angles to the nadir (usually 15°), and rotated in azimuth to look away from the dominant sun glint on the ocean's surface, as long as care is taken to also avoid the direct antisolar point, where aircraft shadow effects become important.

The combination of aircraft altitude, aircraft ground speed, digitization frequency and angular field-of-view, determine the size of the footprint on the ocean surface which is viewed by the MARS. In JGOFS, these parameters were a field-of-view of 10°, altitude of 170 meters, a speed of approximately 130 m/sec, and a sample rate of 0.6 seconds. The average footprint was, therefore, an oval of max/min dimensions of 140 × 60 meters. Because each channel is sampled in sequence before averaging takes place (as opposed to averaging several samples of one channel, and then proceeding to the next), the measurements of a fov at different wavelengths may be taken as being effectively coincident in time.

As part of our effort under this grant, we undertook two engineering upgrades to improve the radiometric performance of the MARS. The first upgrade was the addition of a separate detector unit to measure 4 channels of incident irradiance $E_d(\lambda)$, using a cosine collector mounted on top of the aircraft. The second upgrade involved a redesign to improve the system's SNR by replacing the original MARS flux collector sphere with one having a smaller diameter and walls of greater reflectivity.

3.1 MARS $E_d(\lambda)$ Subsystem Upgrade

When measuring ocean color from low altitude aircraft, it is often desirable (or even necessary) to operate under sky conditions ranging from cloud free to broken overcast to complete overcast. Under these circumstances, any quantitative oceanographic interpretation of the data requires that some account be taken of variations in the magnitude and spectral quality of irradiance incident on the sea surface (Sect. 2 above). In several earlier studies (*e.g.* Mueller 1976; Mueller and Trees 1989), it was necessary for investigators to attempt to model incident irradiance effects empirically, but a better approach is to measure $E_d(\lambda)$ directly (Sect. 2 above).

The original MARS design did not allow for measurement of downwelling spectral irradiance $E_d(\lambda)$. Fortunately, however, the MARS electronic circuits were designed with 4 unused channels, in addition to the 10 spectral radiance channels. It was, therefore, relatively straightforward to add a 4–channel irradiance sensor to the system.

A 3.0 cm diameter Plexiglas diffuser was mounted in a 9.5 cm black anodized aluminum disk, having a raised lip to obscure the diffuser from radiance incident from below the horizon. This cosine collector assembly was mounted on the end of a 7 cm diameter, 17.8 cm long tube of black anodized aluminum. Inside the tube were mounted 4 filter/detector assemblies, identical in design and fabrication to those used to measure radiance through the MARS integrating sphere. The fov of each detector was limited and aligned to view the back surface of the Plexiglas cosine irradiance collector. Mounted with each detector was its associated transimpedance amplifier circuit (converts detector current to voltage). The irradiance sensor is connected to the main MARS electronic circuits, to draw detector power and transmit detector response voltage signals, via shielded cables. This upgrade was successfully completed prior to the MARS MLML/JGOFS (NABE) deployment in April–June 1989.

3.2 MARS Radiance Collector Sphere Upgrade

Although several advantages accrue from the use of an integrating sphere radiance collector in the MARS design (Sect. 3.0 above), there is also a net loss in spectral radiative flux to each detector as a result of absorptive losses in the sphere walls. The flux throughput τ to an exit port is defined as

$$\tau = \frac{\phi_e}{\phi_i}, \tag{19}$$

where ϕ_e is flux through the exit port, and ϕ_i is flux into the sphere. The dependence of τ on reflectance ρ of the sphere wall, sphere diameter D, and port diameter d_e is given approximately as (Goebel 1967)

$$\frac{\phi_e}{\phi_i} = \frac{\rho \, f_e}{1 - \rho(1 - f_t)}$$ (20)

where

$$f_e = \frac{d_e^2}{4D^2} \text{ and}$$ (21)

$$f_t = \frac{(N+1)d_e^2}{4D^2} = (N+1) \, f_e$$ (22)

for a sphere with N exit ports and one entrance port, all of equal diameter d_e.

Clearly, the collector sphere diameter and wall reflectance affect critically the SNR performance of the MARS instrument. The original MARS design implementation was configured with an aluminum sphere of $D_1 = 5$ inches diameter, the interior of which was coated with Barium–Sulfate, which has an approximate reflectance of $\rho_1 = 0.96$.

We consider now the approximated increase in flux to each of the N = 10 detector ports of diameter $d_e = 0.375$–inches, given also one entrance port of the same diameter, were the sphere diameter decreased to $D_2 = 3$ inches, and wall reflectance increased to $\rho_2 = 0.99$. This reflectance increase can be realized by fabricating the sphere from Spectralon. The ratio of exit port fluxes for a fixed input of flux ϕ_i passing through each of two spheres is, from (20),

$$\frac{\phi_{2e}}{\phi_{1e}} = \frac{\rho_2 \, f_{2e}}{\rho_1 \, f_{1e}} \bullet \frac{1 - \rho_1(1 - f_{1t})}{1 - \rho_2(1 - f_{2t})},$$ (23)

where subscript 1 denotes parameters for the original 5–inch Barium–Sulfate coated sphere, and subscript 2 denotes parameters for the smaller sphere. From (21) $f_{1e} = 1.056 \times 10^{-3}$ and $f_{2e} = 2.934 \times 10^{-3}$, and from (22) we have that $f_{1t} = 11f_{1e}$ and $f_{2t} = 11f_{2e}$. Substituting these values and the appropriate sphere reflectances in (23) yields a predicted increase in flux to each detector by a factor

$$\frac{\phi_{2e}}{\phi_{1e}} = 3.49 \, ,$$

if the smaller Spectralon™ sphere were substituted for the initial 5–inch sphere. Assuming that the

---

™ "Spectralon" is a registered trademark of Labsphere, Inc.
    P.O. Box 70
    North Sutton, NH 03260

SNR will increase as flux/$\sqrt{2}$, we may predict that SNR will improve by a factor of approximately 2.5 when this upgrade is installed.

To follow up on the above analysis, Dr. Lange designed and specified a new 3–inch diameter Spectralon™ integrating sphere, including 10 detector ports (0.375 inch diameter) and a 1–inch diameter entrance port (which can be stopped down with a fov limiting aperture). This sphere was custom machined by Labsphere, Inc. and delivered to CHORS in early 1990. Just prior to his death in April 1990, Dr. Lange was in the process of designing new, lower–noise detector circuits and a new mechanical housing to accommodate the new sphere, and he had acquired many of the parts. These additional improvements were not implemented before his death, however, and we have not had resources to reconstruct his unfinished work. The groundwork for this upgrade was nevertheless soundly laid by Dr. Lange, and the second generation MARS can be assembled around the new sphere on relatively short notice, and at low cost. Should a new project emerge which includes use of the MARS system, we need only procure new filter/detector assemblies at appropriate wavelengths, *e.g.* for SeaWiFS or MODIS, install and tune new transimpedance amplifiers, and connect each detector circuit to either the existing (or probably at this date, a more modern) analog–to–digital and data logging system.

4.0 MARS MEASUREMENTS DURING THE JGOFS NORTH ATLANTIC BLOOM EXPERIMENT (NABE) AND AT THE ONR MARINE LIGHT MIXED LAYER (MLML) MOORING SITE IN 1989

In the spring of 1989, Dr. Frank Hoge of NASA WFC headed a flight mission to obtain remote sensing data in the eastern North Atlantic Ocean, in direct support of the JGOFS NABE pilot experiment, and of pre–experiment reconnaissance survey and moored data acquisition work under ONR's MLML program. Dr. Lange was invited to obtain ocean color measurements on this mission using the MARS, both to support ONR's MLML related interests, and to obtain comparisons between data from the MARS and Dr. Hoge's Airborne Oceanographic LIDAR (AOL) system [which includes also a capability for "passive" measurements of upwelled spectral radiance $L(\lambda)$]. Dr. Lange traveled to WFC in April 1989, installed the MARS aboard the P3 aircraft, and participated in several local test flights. He then accompanied the P3 on the complete mission, which extended from late April through early June 1989.

4.1 Mission Summary And Data Inventory

The tracklines flown by the NASA P3 during the JGOFS (NABE)/MLML mission (April–June 1989) are illustrated in Fig. 2, and track segments along which MARS data were acquired are summarized in Table 1. The MARS data files acquired along the various track segments are

---

™ "Spectralon" is a registered trademark of Labview, Inc.
   P.O. Box 70
   North Sutton, NH 03260

catalogued in Table 2, along with comments describing weather conditions, key events and data quality. Track segments corresponding to key data files are annotated in Fig. 2 by the date and letters (*e.g.*, "24 May A, C"); these letters correspond to the last character in the name of the corresponding data file (Table 2).

Under NASA support, Dr. Charles Trees, of CHORS, also participated in the 1989 JGOFS (NABE) and acquired bio-optical profiles at 17 stations aboard the R/V Atlantis II (Fig. 3). Due to adverse weather conditions, none of these *in situ* profiles were made simultaneously with a P3/MARS overflight. Nevertheless, I am collaborating with Dr. Trees in analyzing the *in situ* profiles to obtain bio–optical algorithms for use with the MARS and AOL data. These analyses will be included in a journal manuscript we are preparing in collaboration with Dr. Hoge (WFC) and Mr. Robert Arnone (NRL/SSC).

4.2   MARS Calibration During the MLML/JGOFS (NABE) Deployment

In preparation for its deployment in April–June 1989, the MARS radiance channels were calibrated both at CHORS (using a lamp standard of spectral irradiance with a reflectance plaque) and at NASA Goddard Space Flight Center (GSFC) (using GSFC's hemisphere radiance source). During the P3 mission, field calibration checks were made, using a portable integrating sphere source belonging to WFC, on the day of each flight. Finally, the MARS $L(\lambda)$ channels were recalibrated at GSFC immediately following the P3's return to WFC, prior to Dr. Lange's return to San Diego.

The MARS $E_d(\lambda)$ were calibrated by Dr. Lange at CHORS, before and after the deployment, using lamp standards of spectral irradiance on a photometric bar.

Dr. Lange carefully evaluated the results from this entire sequence of laboratory and field calibrations of the MARS absolute responsivity for each channel. The results of this analysis are summarized in Table 3.

The calibration coefficients in Table 3 were then applied, by Dr. Lange, to the MARS raw data files (Table 2) from several of the tracklines illustrated in Fig. 2. He also merged the P3 navigation records, received from WFC, with the calibrated data. These calibrated trackline data sets were stored on MS/DOS floppy disks, and following Dr. Lange's death, we were able to locate some, but not all, of them. Furthermore, a student who was working on critical selected track segments removed the only copies of several MS/DOS disks containing the calibrated data (he wished to work on the data on campus using a PC in his office). The student then left the San Diego area, leaving no forwarding address, and we have been unable to locate several critical segments of the calibrated data [and in particular the segments which are best suited for analyses of our normalization model, Eq. (18), see 4.3 below]. The situation is recoverable by simply reprocessing the raw data files to apply calibration coefficients (Table 3) and merge the P3 navigation data. However, I am unable to include examples of our preliminary atmospheric correction analyses with this report. These results will appear in a

12

journal manuscript which I and my collaborators at CHORS, WFC and NRL expect to complete within a few months.

4.3 Correction and Normalization of MARS Spectral Radiance with Incident Spectral Irradiance

We introduced in Sect. 2.0 above a method for normalizing low altitude measurements of spectral ocean color radiance ratios $L(\lambda_1)/L(\lambda_2)$ using estimates of ratios of incident irradiance $E_d(\lambda_2)/E_d(\lambda_1)$, and to also correct the data for skylight reflected at the surface and (small) atmospheric transmittance effects [Eq. (17)]. Chlorophyll a concentration is then estimated using the normalized water–leaving radiance estimates in an algorithm similar to Eqs. (11) and (12). We now consider the sensitivity of derived chlorophyll a to the accuracy with which $\varsigma(\lambda, \lambda_r)$ estimates parameterize the spectral quality of incident irradiance in Eq. (17).

Figure 4 compares estimated distributions of chlorophyll a concentration calculated from the MARS data using two different methods for estimating $\varsigma(\lambda, \lambda_r)$, along a short segment of tracklines E–F on 21 May 1989 (Fig. 2). This data segment was selected for analysis because approximately the first half (left side of Fig. 4) was measured under cloud–free skies, and the remainder was taken under complete overcast (except for a brief stretch of broken cloud cover near the edge of the cloud deck). The chlorophyll a profile illustrated by the dashed curve was computed using fixed nominal values of $\bar{\varsigma}(\lambda, \lambda_r)$, which were estimated by averaging $E_d(\lambda)/E_d(\lambda_r)$ measurements for the day to simulate the best approximation one might hope for using a regional climatology. The chlorophyll a estimates represented by the solid curve in Fig. 4 were calculated by normalizing the MARS radiance ratios with $\varsigma(\lambda, \lambda_r)$ [Eq. (9)], estimated using simultaneously measured ratios $E_d(\lambda)/E_d(\lambda_r)$ directly, with no attempt to correct for the spatial dislocation of the MARS "footprint" and the sensor located on top of the aircraft [see the discussion in Sect. 2.0 leading to Eq. (18)].

In this preliminary analysis, chlorophyll a concentrations were derived using an algorithm derived from shipboard measurements of $L_u(\lambda)$, $E_d(\lambda)$ and chlorophyll a (determined using HPLC methods) which were taken during May and June 1987 in the Greenland Sea. (Mueller and Trees 1989). This algorithm was formulated in terms of ratios of reflectance $R_L(\lambda)$ [Eq. (13)] as

$$C = 3.33 \left[\frac{R_L(440)}{R_L(550)} \right]^{-1.93} . \tag{23}$$

Normalization in terms of reflectance represents an intermediate step in the transition from the use of water–leaving radiance $L_w(\lambda)$ to normalized water–leaving radiances $L_{wN}(\lambda)$ in ocean color algorithms (Gordon 1990; Mueller and Austin 1992). The model for estimating reflectance ratios is similar to Eq. (17), but does not include the normalization to extraterrestrial solar flux. We may thus derive an expression for estimating reflectance ratios $R_L(\lambda_1)/R_L(\lambda_2)$ from MARS radiances by multiplying both sides of Eq. (17) by $F(\lambda_2)/F(\lambda_1)$, which yields

13

$$\frac{R_L(\lambda_1)}{R_L(\lambda_2)} = \frac{\left[t^{-1}(\lambda_1,\mu) \ L(\lambda_1) - \varsigma(\lambda_1,\lambda_r) \ L(\lambda_r)\right] \varsigma(\lambda_2,\lambda_r)}{\left[t^{-1}(\lambda_2,\mu) \ L(\lambda_2) - \varsigma(\lambda_2,\lambda_r) \ L(\lambda_r)\right] \varsigma(\lambda_1,\lambda_r)} . \tag{24}$$

Equations (17) and (24) are entirely equivalent, within the constant scale factor $F(\lambda_1)/F(\lambda_2)$, and Eq. (23) is equivalent to an algorithm based on normalized water–leaving radiances within the constant scale factor $[F(440)/F(550)]^{-1.93}$.

The comparison in Fig. (4), between the nominal and measured $E_d(\lambda)$ ratio normalization, shows clearly how failure to account for actual variations in the spectral quality of incident irradiance may create artificial patterns of variability in estimated chlorophyll a concentration. In this case, the nominal irradiance ratio values also bias the chlorophyll a estimates positively for all cloud conditions.

In additional regression analyses of this particular data set (not shown here), we found that $E_d(725)$ was significantly and linearly correlated with $L_u(725)$ over a moving, alongtrack window of approximate 30 second duration, and that ratios $E_d(\lambda)/E_d(725)$ [$\lambda = 409$, 438 and 549 nm] were each, in turn, linearly correlated with $E_d(725)$ over the same windows. These results suggest that improved estimates of $\varsigma(\lambda,\lambda_r)$ (compared to the simultaneous ratios) can be obtained from $L_u(725)$ using a quadratic form of Eq. (18), with time dependent coefficients. These analyses were performed by a student working under my direction. Unfortunately, the student left the San Diego area without leaving a forwarding address, and we have been unable to locate him, the calibrated form of the trackline data, or the results of his analyses. This work, must be repeated after I have recalibrated the original data and merged it with the P3 navigation records. We will then compare the resulting pigment estimates with those derived from the AOL, the accuracy of which is not sensitive to $E_d(\lambda)$ variations, and evaluate the accuracy of atmospheric corrections and normalizations quantitatively.

4.4 Mesoscale Variability in Chlorophyll Concentrations Estimated from MARS Observations in the Eastern North Atlantic Ocean (18 May through 3 June 1989)

Figures 5 through 8 illustrate mesoscale variability in chlorophyll a distributions estimated from the MARS measurements along several of the P3 tracklines illustrated in Fig. 2.

Figure 5 shows chlorophyll a variability on 18 May 1989 along the transect from Shannon, Ireland to the position of the R/V Atlantis II in the JGOFS NABE sampling grid near 47°N, 20°W (18 May A, C, Fig. 2). Figure 6 illustrates estimated chlorophyll a variability on 18 May along 20°W longitude between 47°N and 49.5°N latitude (18 May D, Fig. 2). The total trackline distance over which chlorophyll a variability is illustrated in Fig. 5 is approximately 800 Km, and that in Fig. 6 is approximately 270 Km. Both tracklines show eddy–like features, characterized by patterns of chlorophyll a variability scales of 50 to 200 Km. The trackline from Ireland to 47°N, 20°W (Track A, C) is characterized by a large scale monotonic increase in chlorophyll a concentration from ~0.5 mg m^{-3} near the Irish coast to ~3 mg m^{-3} near the JGOFS NABE site; meridional variability along

14

20°W (Track D) is characterized by variability of much smaller amplitude, with concentrations hovering near 1 mg m^{-3}.

Chlorophyll a variability further to the north along the 20°W meridian, as measured with the MARS on 21 May 1989 during the P3 transmit from Shannon, Ireland to Reykjavik, Iceland (21 May D and E, Fig. 2), is illustrated in Fig. 7; this segment of the 21 May 1989 trackline was essentially cloud free in its entirety, and the transition to overcast conditions (illustrated in Fig. 4) occurred further north along track segment F (see Fig. 2). This trackline is characterized by a single, low–chlorophyll, clear–water feature near 53°N, with scale $\geq$200 Km. Chlorophyll a variability on 21 May 1989 between 55°N and 60°N along 20°W is similar to that observed on 18 May 1989 between 47° and 49.5°N (Fig. 6), $i.e.$ values hover near 1 mg m^{-3}, with weak eddy–like variability features having dominant scales between 50 and 100 Km. The northern part of this transect ends near the sites of the JGOFS and MLML moorings.

Figure 8 illustrates the distributions of chlorophyll a between 60°N and Iceland (~64°N) on 29 May and 3 June 1989. This segment is characterized, on both days by several eddies, with horizontal scale of order 50 Km, which have significantly larger amplitudes (0.5 to 2 mg m^{-3}) than were observed south of 60°N (~0.25 mg m^{-3}; Fig. 7). These features were interpreted by Dr. Lange, with the aid of his visual observations, as mesoscale eddies which gave the appearance of forming near the coast of Iceland and propagating southward through the period. It is also noteworthy, that although the amplitude of bio–optical variability northward from the MLML mooring appears to increase somewhat through this period, values seem to persistently hover near 1 mg m^{-3} at the mooring site itself.

4.5 Bio–Optical Characteristics of an Ocean Front over the Iceland–Faeroe Ridge

On 25 May 1989, the NASA P3 flew transects to map bio–optical variability over the continental shelf off the southern coast of Iceland, and over the Iceland–Faeroe Ridge, which topographically isolates the intermediate and deep water masses of the Norwegian and North Atlantic basins. The P3 tracklines covered on this sortie are sketched in Fig. 9 (tracklines are labeled 1A through 1G, and 2, 5, and 8–10); Fig. 9, presented courtesy of Dr. Frank Hoge, of NASA WFC, also illustrates the relative distribution of chlorophyll a estimated from AOL fluorescence along each trackline ("stick" height is proportional to chlorophyll a concentration).

Figure 10 compares the relative chlorophyll distributions measured by the MARS and the AOL along Trackline 1B (Fig. 9), which transects from south–to–north across a strong bio–optical front near 64.5°N; also shown in Fig. 10 is the profile of Sea Surface Temperature measured from the P3 using an infrared radiation thermometer. The MARS and AOL chlorophyll traces were arbitrarily offset to facilitate comparison. Figure 10 was prepared by Dr. Lange, prior to his death, and I can find no documentation explaining the details of the algorithm he used to derive the MARS chlorophyll trace shown here. However, we do have the calibrated MARS data he prepared for these

tracklines and re–analysis will be relatively straightforward. In any event, the MARS and AOL relative estimates agree remarkably in every detail (Fig. 10). Dr. Trees and I will revisit this data set soon to include it in the journal manuscript we intend to publish jointly with Dr. Frank Hoge of NASA WFC and Mr. Robert Arnone of NRL/SSC, who also accompanied this P3 mission and has analyzed the infrared sea surface temperature data and AXBT vertical temperature profiles recorded along these flightlines.

5.0 SUMMARY AND CONCLUSIONS

This final report formally competes our performance under ONR Grant N00014–89–J–1468. We successfully completed one engineering upgrade to the MARS by implementing uplooking channels to measure incident spectral irradiance $E_d(\lambda)$ (Sect 3.1 above). We partially completed a second upgrade, to increase the system's SNR by installing a smaller, more–reflective integrating sphere for radiance collection; the actual installation of the sphere was forestalled by the death of my Co–Principal Investigator, Dr. Ed Lange, and we have therefore simply held the parts pending a future time when a new deployment of the MARS may be proposed (Sect. 3.2).

Dr. Lange also successfully completed MARS measurements of bio–optical variability near the ONR MLML mooring (near 60°N, 20°W) and the JGOFS/NABE stations along 20°W in the North Atlantic Ocean. These measurements were made aboard the NASA WFC P3 aircraft between late April and early June 1989. The analyses and publication of scientific results from these MARS measurements were also severely disrupted by Dr. Lange's death. Indeed, we were able to recover very few of the calibrated radiance/irradiance data files which Dr. Lange prepared from the raw MARS data. Fortunately, we do retain both the original data and the results of Dr. Lange's radiometric calibrations of the MARS, and we expect to be able to fully reconstruct this work, complete the analyses, and publish the results in a referenced journal.

In order to bring this work to a scientifically satisfactory conclusion, I (together with Dr. Trees of CHORS, Dr. Hoge of NASA WFC and Mr. Arnone of NRL/SSC) intend to recalibrate the MARS trackline segments discussed above, and merge each file with the associated P3 navigation records and AOL data. Pigment and K(490) algorithms will be derived in collaboration with Dr. Trees, from his *in situ* bio–optical profile measurements aboard the Atlantis II (Sect. 4.1 and Fig. 3). These algorithms will be applied to the MARS data, and we will then proceed to complete the analyses outlined and described above in Sects. 2 and 4.

I would have preferred to complete this analysis and manuscript preparation prior to submitting this Final Technical Report, but the grant period has too long expired. We will, of course, provide ONR representatives with copies both of a preprint of the manuscript (as submitted), and reprints after the article appears in a referred journal, and acknowledge this grant as supporting my contributions. My colleagues and I plan to submit this manuscript within the next few months, hopefully for publication in late 1993 or early 1994.

16

REFERENCES:

Austin, R.W. and T.J. Petzold, 1981. The determination of the diffuse attenuation coefficient of sea water using the coastal zone color scanner. In: J.F.R. Gower, (Ed.), *Oceanography from Space,* Plenum, N.Y. pp. 239–256.

Cox, C. and W. Munk, 1954. Measurement of the roughness of the sea surface from photographs of the sun's glitter. J. of the Opt. Soc. of Am. **44**(11): 838–850.

Goebel, D.G., 1967. Generalized integrating sphere theory. Appl. Opt., **6**: 125.

Gordon, H.R., D.K. Clark, J.W. Brown, O.B. Brown, R.H. Evans, and W.W. Broenkow, 1983. Phytoplankton pigment concentrations in the middle Atlantic Bight: comparison of ship determinations and CZCS estimates. Appl. Opt. **22**(1): 20–36.

Gordon, H.R., 1990. Radiometric considerations for ocean color remote sensors. Appl. Opt., **29**: 3228–3236.

Hoge, F.E. and R.N. Swift, 1993. The influence of chlorophyll pigment on upwelling spectral radiances from the North Atlantic Ocean: an active–passive correlation spectroscopy study. Deep–Sea Res. II., **40**: 265–277.

Mueller, J.L., 1974. *The Influence of Phytoplankton on Ocean Color Spectra.* Ph.D Thesis, Oregon State University, Corvallis. 239 p.

Mueller, J.L., 1976. Ocean color spectra measured off the Oregon coast: characteristic vectors. Appl. Opt., **15**(2): 394–402.

Mueller, J.L. and R.W. Austin, 1992. *Ocean Optics Protocols for SeaWiFS Validation.* NASA Tech. Memo. 104566, Vol. 5. 45pp.

Mueller, J.L. and C.C. Trees, 1989. *Bio–Optical Variability in the Greenland Sea Observed with the Multispectral Airborne Radiometer System (MARS) (21 May–2 June 1987).* CHORS Tech. Memo. TM 90–001. SDSU/CHORS, San Diego, CA 81p + Appendices.

Neckel, H. and D. Labs, 1984. The solar radiation between 3300 and 12500A. Solar Phys. **90**. 205-258.

Table 1

Summary of MARS Data Acquisition Along NASA P3 Tracklines Flown During the JGOFS North Atlantic Bloom Experiment and at the ONR MLML Mooring Site in May and June 1989

Flight Date	Track Location	Data Coverage (%)	Data Quality (1)
4/25/89	transit Lajes/Shannon over 45°N mooring	40	2 to 3
5/02/89	Shannon/45°N mooring	80	1 to 2
5/10/89	Shannon/45°N mooring	50	1 to 3
5/17/89	Shannon/45°N mooring	< 5	4
5/18/89	Shannon/45°N mooring	80	2
5/21/89	xsit Shannon/Keflavik over 60°N/MLML mooring	100	1 to 3
5/22/89	Keflavik/Greenland MIZ	100	1
5/24/89	Kefl/60°N/MLML	100	1 to 3
5/25/93	Kefl/Iceland Faeroe ridge	100	1
5/29/89	Kefl/MLML/60°N mooring	100	1
6/03/89	Kefl/MLML/60°N mooring	100	1 to 4

Notes:
(1) Data Quality Key: 1: clear sky   2: broken clouds   3: complete overcast 4: undercast and fog

Table 2: MARS JGOFS (NABE)/MLML Data File

Directory of MARS data files and synopsis extracted from Dr. Lange's field notes, recorded aboard the NASA WFC P3 aircraft during MARS survey runs over the JGOFS (NABE) and MLML experiment sites in May and June 1989.

File Name	Data Type	File Size (Bytes)	Date of Acquisition	End Time	Weather/Comments
JGOFS 1					
042089A	CRD	544	4-20-89	4:32p	xsit Wallops/St Johns
042189A	BIN	230369	4-20-89	5:13p	clear
042089B	BIN	205483	4-20-89	5:49p	clear
042089C	BIN	139473	4-20-89	6:14p	clear
JGOFS2					
042189A	CRD	554	4-21-89	11:56a	xsit St John/Lejes
042189A	BIN	99039	4-21-89	12:40p	clear first third
042189B	BIN	209899	4-21-89	1:56p	fog
042189C	BIN	52763	4-21-89	2:44p	rain
042189D	BIN	230231	4-21-89	4:35p	broken overcast
JGOFS3					
042489A	CRD	555	4-24-89	11:41a	first JGOF mooring
042489A	BIN	231059	4-24-89	12:21p	bad data?? cloudy
042489B	BIN	234233	4-24-89	1:02p	sun glint is bad-no signal
JGOFS4					
042589A	CRD	552	4-25-89	12:31p	xsit Lajes/Shannon
042589A	BIN	230599	4-25-89	1:28p	sounding-clear
042589B	BIN	200055	4-25-89	2:18p	good AOL/MARS comparisons
042589C	BIN	186255	4-25-89	3:04p	good AOL/MARS comparisons
JGOFS5					
CALIB	CRD	532	5-02-89	9:59a	
CALIB	BIN	6717	5-02-89	10:06a	
CLOUDS	CRD	549	5-02-89	11:28a	
CLOUDS	BIN	7039	5-02-89	11:30a	
050289A	CRD	525	5-02-89	1:49p	first ship crossing mooring 45°N
050289A	BIN	230507	5-02-89	2:41p	good weather-MARS/AOL day
050289B	BIN	159345	5-02-89	3:17p	good weather-MARS/AOL day

File Name	Data Type	File Size (Bytes)	Date of Acquisition	End Time	Weather/Comments
JGOFS6					
SPHERE	CRD	513	5-10-89	9:42a	
DARK	BIN	4923	5-10-89	9:08a	
SPHERE	BIN	4739	5-10-89	9:43a	sphere burned one bulb!
051089A	CRD	523	5-10-89	10:44a	50% coverage/clouds
051089A	BIN	248815	5-10-89	11:43a	JGOFS 45°N Discovery
051089B	BIN	220525	5-10-89	12:33p	rec 800-1200 good wx
051089C	BIN	143567	5-10-89	1:07p	windrows...
JGOFS7					
051089D	BIN	151893	5-10-89	1:42p	patchy, irregular illumination
051089D	CRD	543	5-10-89	1:45p	
051089E	BIN	242651	5-10-89	2:39p	same
051089F	BIN	14208	5-10-89	2:44p	30 sec of zero values
JGOFS8					
SPHERE	CRD	527	5-17-89	9:49a	
051789A calibration	CRD	516	5-17-89	11:49a	fogged out this day-good
SPHERE	BIN	11823	5-17-89	10:25a	
RIVER	BIN	98073	5-17-89	11:34a	interesting data set
051789A	BIN	11685	5-17-89	11:52a	
051789B	BIN	23507	5-17-89	12:00p	
JGOFS9					
CALIB	CRD	518	5-18-89	9:00a	
DARK1	BIN	4785	5-18-89	9:02a	dark value study
DARK2	BIN	4647	5-18-89	9:28a	
SPHERE	BIN	10351	5-18-89	9:45a	sphere burned one bulb-reassem
051889A	CRD	564	5-18-89	11:15a	
GULF	BIN	45541	5-18-89	10:40a	
CLOUDS	BIN	11823	5-18-89	10:47a	
051889A	BIN	230369	5-18-89	12:06p	patchy chlor *a* - patchy sky
051889B	BIN	98901	5-18-89	12:29a	
JGOFS10					
051889C	BIN	207967	5-18-89	1:16p	patchy chlor *a* - patchy sky
051889D	BIN	102075	5-18-89	1:40p	
051889E	BIN	218409	5-18-89	2:29p	
051889F	BIN	32523	5-18-89	2:45p	

File Name	Data Type	File Size (Bytes)	Date of Acquisition	End Time	Weather/Comments
JGOFS11					
052189A	CRD	535	5-21-89	11:03a	xsit Shannon/Keflavik
SPHERE	BIN	9937	5-21-89	9:41a	
DARK	BIN	4831	5-21-89	10:03a	
DARK2	BIN	75441	5-21-89	10:58a	
052189A irradiance	BIN	188417	5-21-89	11:45a	smoggy-lot of path
052189B	BIN	25163	5-21-89	11:52a	bright/dark/bright/...
052189C	BIN	73601	5-21-89	12:10p	10% useful
052189D	BIN	233221	5-21-89	1:03p	best passive run AOL/MARS
JGOFS12					
052189E	BIN	235245	5-21-89	1:57p	continue with excellent day
052189F	BIN	233589	5-21-89	2:50p	cloudy/rain
052189G	BIN	126593	5-21-89	3:20p	rain/inclement
JGOFS13					
052289A	CRD	550	5-22-89	2:07p	Nancy's ice mission
SPHERE	BIN	17021	5-22-89	2:00p	
052289A	BIN	244307	5-22-89	3:28p	clear to excellent
052289B	BIN	242145	5-22-89	4:27p	
052289C	BIN	189889	5-22-89	5:14p	
JGOFS14					
052289D	BIN	237867	5-22-89	6:15p	
052289E	BIN	33995	5-22-89	6:24p	
JGOFS17					
052489A	CRD	548	5-24-89	11:02a	MLML second survey
052489A	BIN	227931	5-24-89	11:48a	good signal, clear wx
SPHERE	BIN	9891	5-24-89	10:05a	
052489B	BIN	230323	5-24-89	12:45p	intermittent sky with rain shws
052489C	BIN	97429	5-24-89	1:10p	

File Name	Data Type	File Size (Bytes)	Date of Acquisition	End Time	Weather/Comments
JGOFS18					
COMMAND	COM	23791	12-30-85	12:00p	
052489D	BIN	235843	5-24-89	2:09p	
052489E	BIN	150513	5-24-89	2:46p	
052489F	BIN	155619	5-24-89	3:25p	
052489G	BIN	55293	5-24-89	3:51p	clearing back to coast
JGOFS21					
052589A islands	CRD	529	5-25-89	11:04a	color front Iceland/Faeroe
052589A	BIN	237223	5-25-89	11:56a	clear wx, exlnt signal
SPHERE	BIN	18171	5-25-89	9:47a	
052589B	BIN	240949	5-25-89	12:51p	clear wx, exlnt signal, some clouds
052589C	BIN	183357	5-25-89	1:33p	
JGOFS22					
052589D	BIN	146971	5-25-89	2:07p	
052589E	BIN	139013	5-25-89	3:37p	
052589F	BIN	84319	5-25-89	3:57p	
DARK	BIN	13939	5-25-89	4:01p	
JGOFS25					
SPHERE	CRD	528	5-29-89	9:38a	
SPHERE	BIN	9247	5-29-89	9:40a	
052989A	CRD	540	5-29-89	12:29p	MLML survey #3
052989A	BIN	230599	5-29-89	1:24p	excellent skies - good day
052989B	BIN	231657	5-29-89	2:16p	intermittent clouds
052989C	BIN	195225	5-29-89	3:01p	into fog
JGOFS26					
052989D	BIN	245917	5-29-89	3:57p	10,000 feet
052989E	BIN	93473	5-29-89	4:19p	good sounding

File Name	Data Type	File Size (Bytes)	Date of Acquisition	End Time	Weather/Comments
JGOFS27					
060389A	CRD	527	6-03-89	9:58a	MLML survey #4
SPHERE18	BIN	9339	6-01-89	8:45a	canceled day
SPHERE17	BIN	9339	5-30-89	7:46a	canceled day
DRIFT	BIN	69691	6-02-89	9:17a	
SPHERE19	BIN	9431	6-03-89	9:38a	sphere behaved badly
060389B	BIN	233037	6-03-89	12:02p	aperture opened
060389A	BIN	241133	6-03-89	11:08a	good wx here, bad later
JGOFS28					
COMMAND	COM	23791	12-30-85	12:00p	
060389C	BIN	243203	6-03-89	12:58p	continue with survey
060389D	BIN	233221	6-03-89	1:51p	

Table 3

MARS Calibration Factors and Effective Wavelengths during the JGOFS (NABE)/MLML
Deployment on NASA's P3 Aircraft in May and June 1989

Channel Number	Variable	Effective Wavelength [nm]	HPFW Bandpass [nm]	Calibration Factor (1) [V μW^{-1} cm^2 sr nm]
1	L	408.6	13.9	0.0037
2	L	437.5	11.3	0.0077
3	L	486.8	10.5	0.031
4	L	518.6	10.0	0.026
5	L	548.8	9.9	0.056
6	L	586.3	12.1	0.089
7	L	629.8	13.0	0.103
8	L	665.6	13.8	0.115
9	L	679.6	14.4	0.125
10	L	726.4	19.0	0.104
				[V μW^{-1} cm^2 nm]
11	E_d	409	14	0.0114
12	E_d	438	11	0.00135
13	E_d	549	10	0.00424
14	E_d	726	19	0.01136

Notes:

(1) Divide MARS voltages by the calibration factor to obtain radiance, or irradiance, for each channel in the units indicated.

MARS
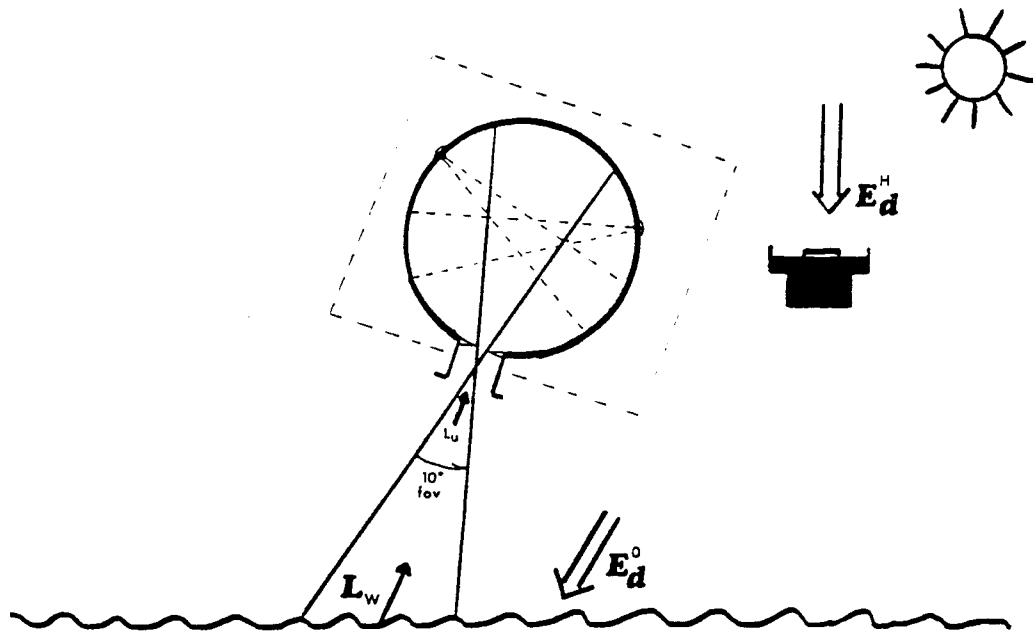
Fig. 1. Schematic illustration of the MARS design concept. Radiance enters the integrating sphere through the entrance lens and field limiting aperture, and is diffusely reflected several times before entering one of the 10 filtered detectors. Each detector views an area, as shown by dotted lines, on the opposite wall of the sphere which avoids viewing the area first illuminated by input flux and the locations of the other detector ports. Incident spectral irradiance at 4 wavelengths is measured via a Plexiglas cosine-collector mounted on top of the aircraft.
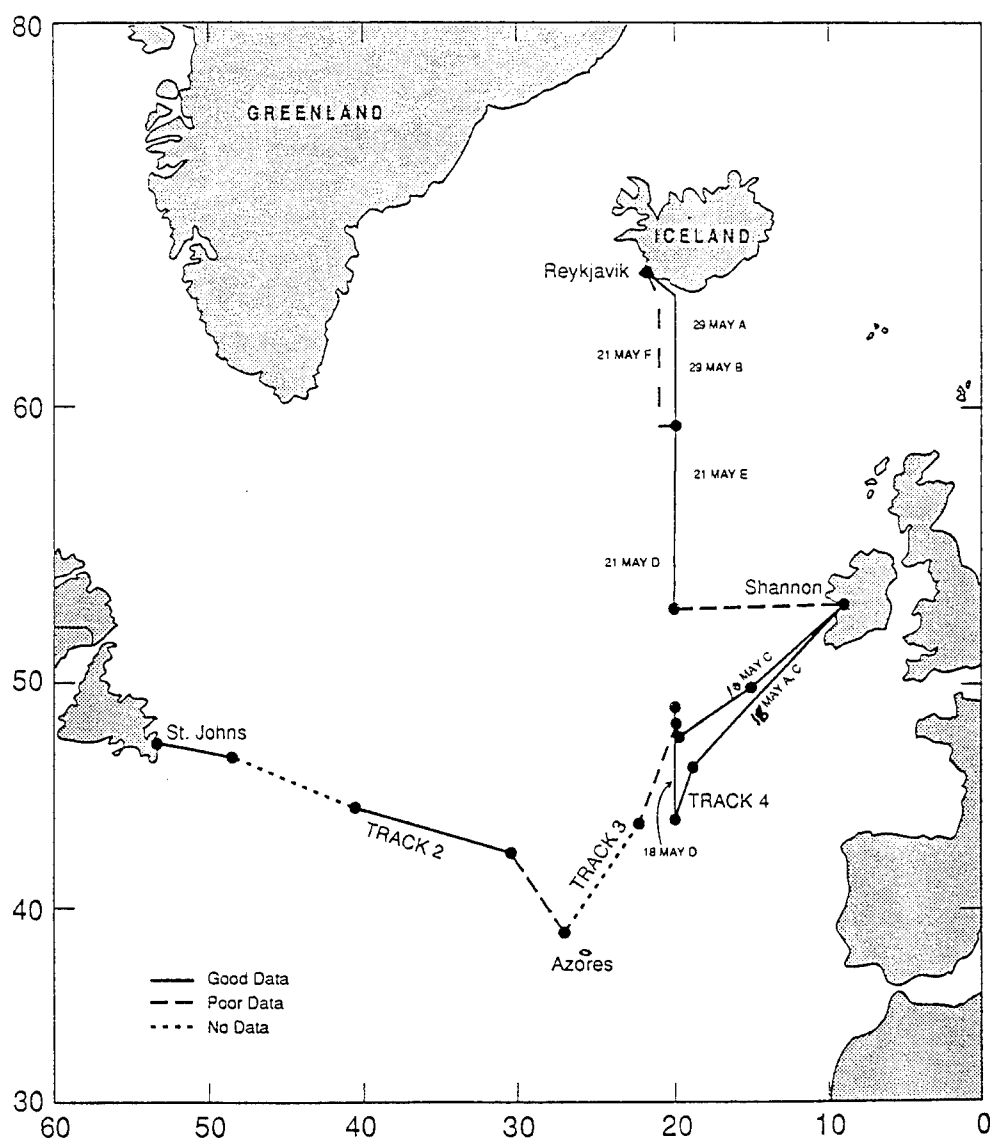
Fig. 2. Locations of key flightlines where MARS data were acquired during late April through early June in 1989, aboard the NASA WFC P3 remote sensing aircraft. This mission supported the JGOFS North Atlantic Bloom Experiment, survey work near ONR's Marine Light-Mixed Layer bio–optical mooring at 60°N, 20°W, and mapping of ocean fronts over the Iceland-Faeroe Ridge in collaboration with the U.S. Navy.
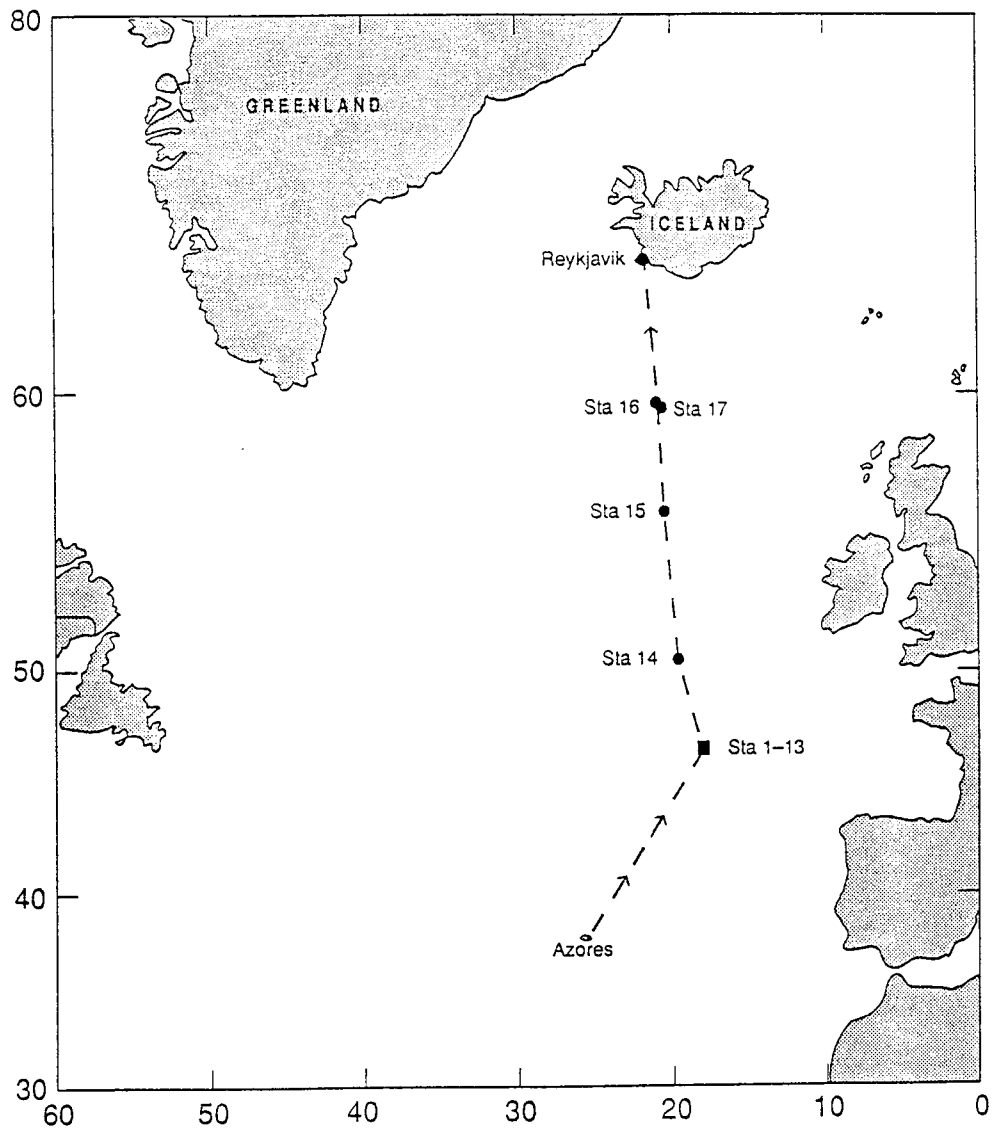
Fig. 3. Locations of 17 stations where vertical profiles of spectral irradiance and radiance, chlorophyll *a* fluorescence and beam transmission at 660 nm were measured by Dr. Charles Trees (also of CHORS) aboard the R/V Atlantis II during the JGOFS NABE (May-June 1989). This work by Dr. Trees, who is collaborating in our analyses of the combined in-water and MARS data set, was independently supported by NASA.

MARS PIGMENT ESTIMATES WITHOUT & WITH UPLOOKING SENSOR
Nominal Ed Ratios — — —
Measured Ed Ratios _____
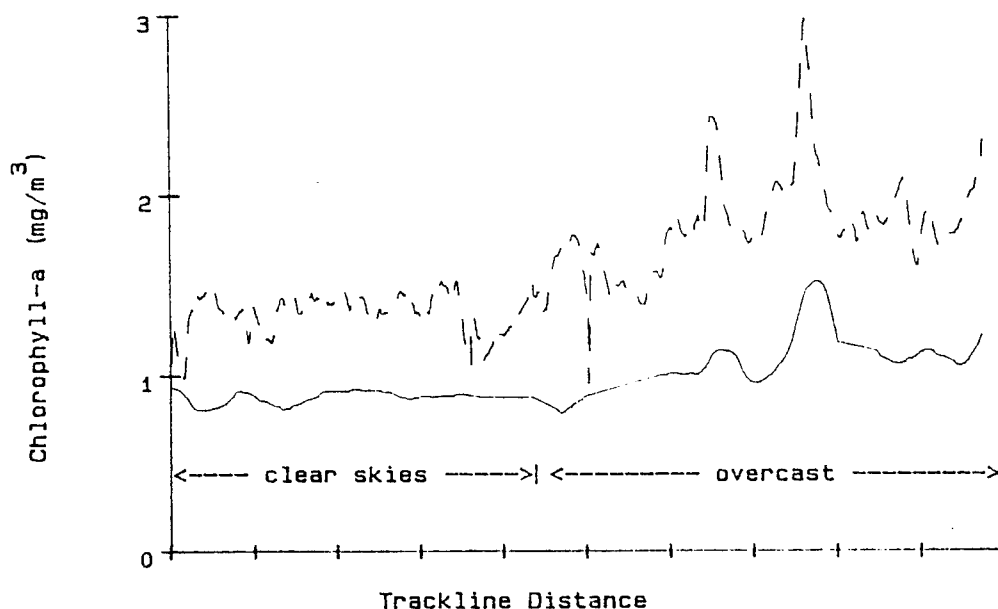
Fig. 4. Comparison of the MARS chlorophyll a estimates obtained using two different methods of incident spectral irradiance normalization. The MARS data were recorded on 21 May 1989 during a brief segment of the coverage from tracklines E and F (Fig. 2). The southern portion of this segment (left subsegment, as marked) was flown under cloud–free skies. The northern part of this data segment was flown under solid overcast. The dashed curve illustrates chlorophyll a estimates calculated using atmospheric corrections and spectral irradiance normalization factors based on constant, nominal regional estimates of "typical" ratios of incident spectral irradiance. The solid curve represents the same calculation based on corrections and normalization using downwelling irradiance measurements from the MARS sensors on top of the aircraft.

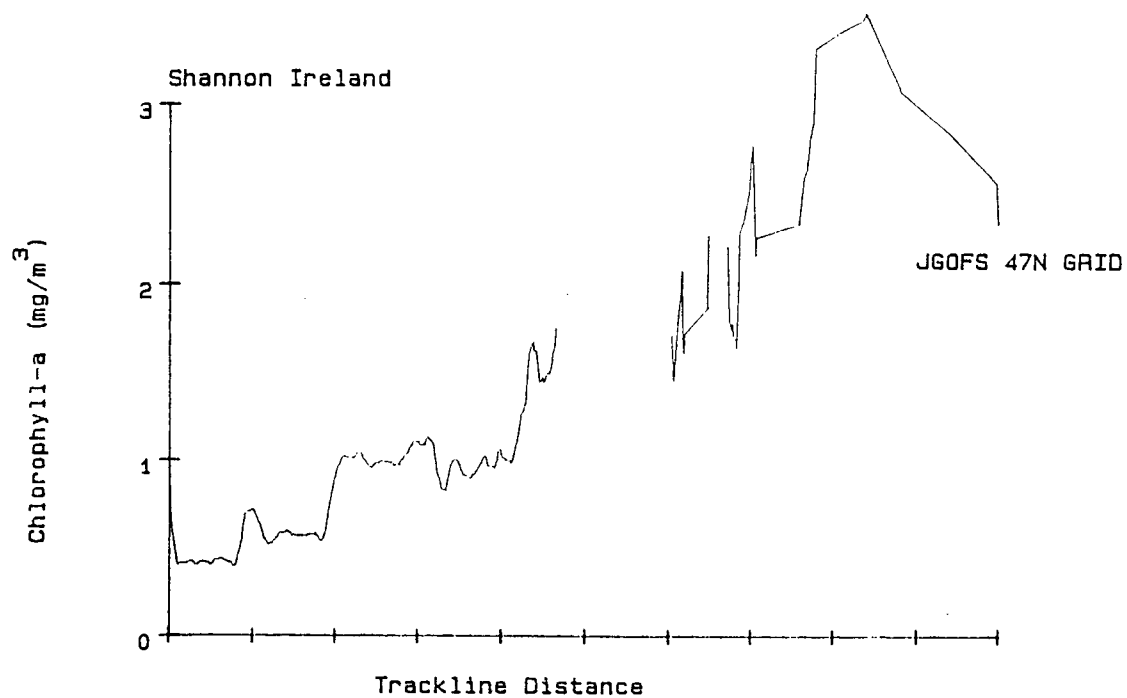28

MARS PIGMENT ESTIMATES
18 May 1989, Tracks A & C

Fig. 5. MARS chlorophyll a estimates along the trackline extending from Shannon, Ireland to the Atlantis II position in the JGOFS grid near 47°N, 20°W on 18 May 1989 (tracklines A - C, Fig. 2).
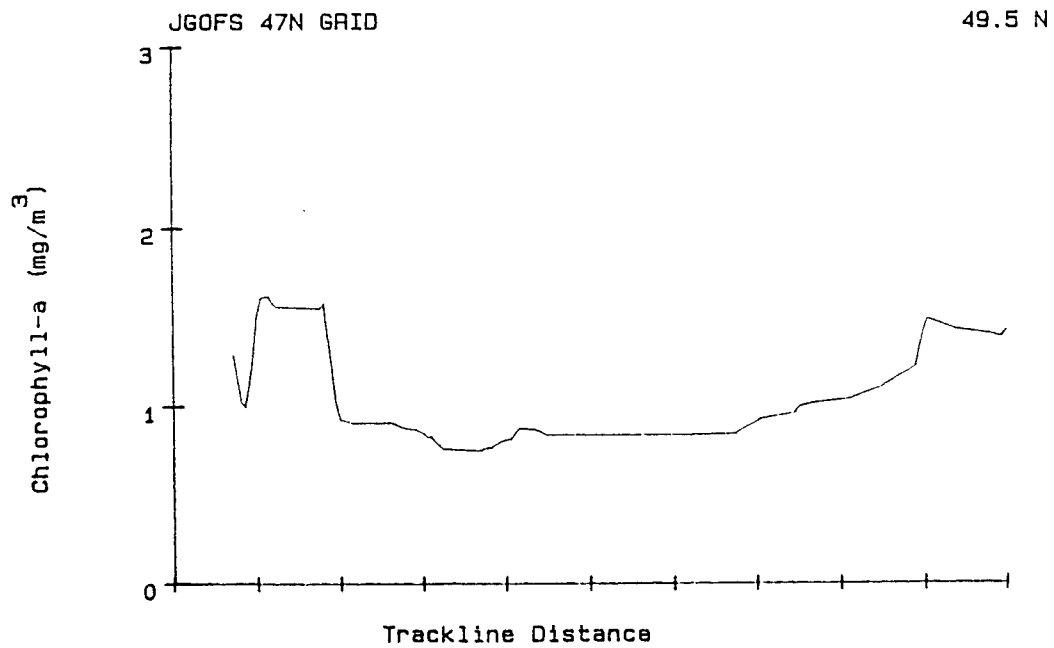
Fig. 6. MARS chlorophyll *a* estimates along the trackline extending along 20°W from 47°N to 49.5°N on 18 May 1989 (trackline D, Fig. 2).

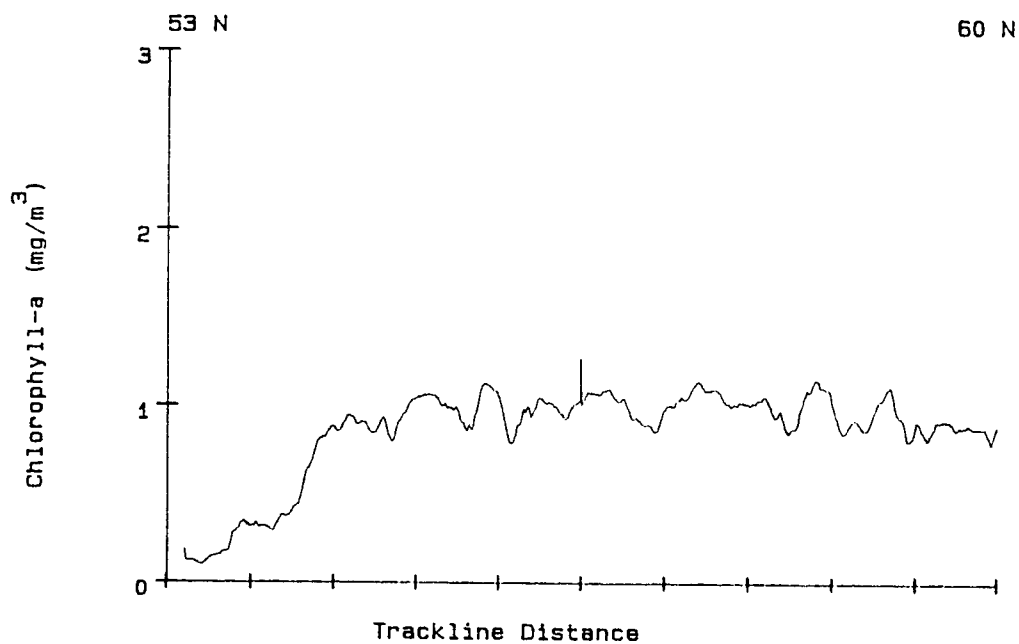MARS PIGMENT ESTIMATES
21 May 1989, Tracks D & E

Fig. 7. MARS chlorophyll *a* estimates along the trackline extending along 20°W from 53°N to 60°N on 21 May 1989 (tracklines D and E, Fig. 2).
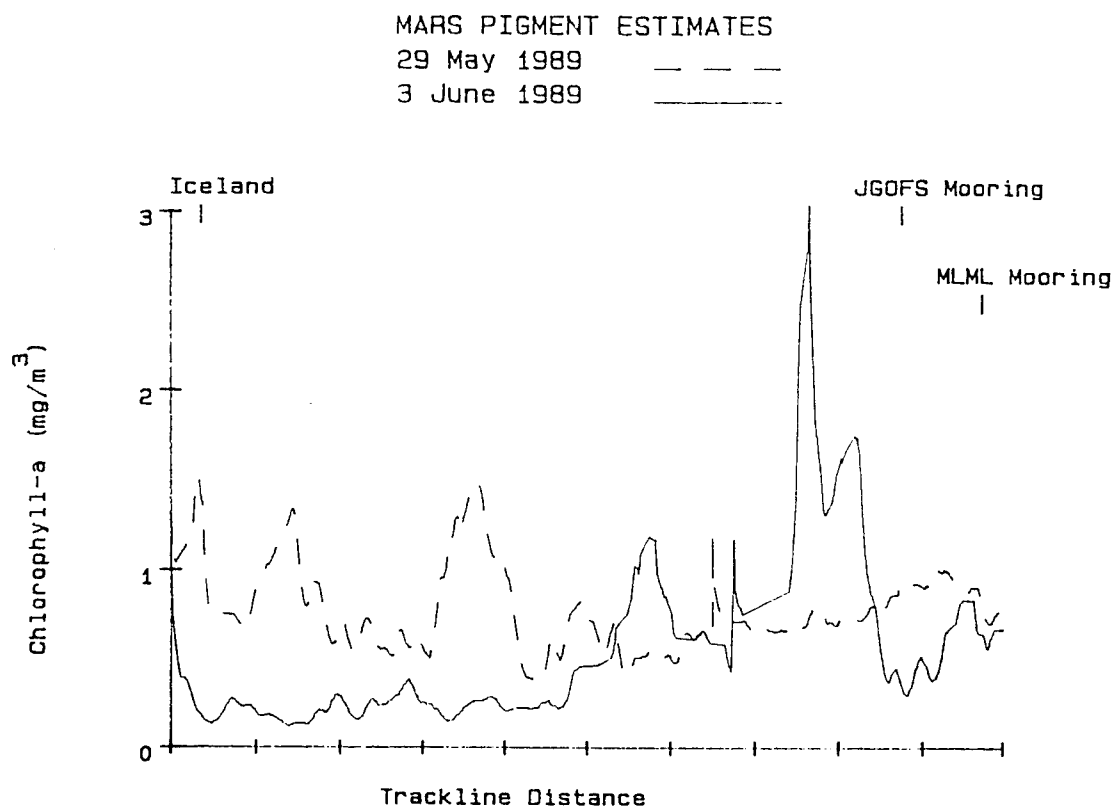
MARS PIGMENT ESTIMATES
29 May 1989   — — —
3 June 1989   _____

Fig. 8. MARS chlorophyll *a* estimates along the trackline extending along 20°W from Iceland to 60°N on 29 May 1989 (tracklines A and B, Fig. 2) and during repeated coverage along this trackline on 3 June 1989. The chlorophyll *a* traces are illustrated by the dashed curve for 29 May and the solid curve for 3 June 1989. The approximate locations of the JGOFS and MLML oceanographic moorings along this trackline are indicated in the figure.
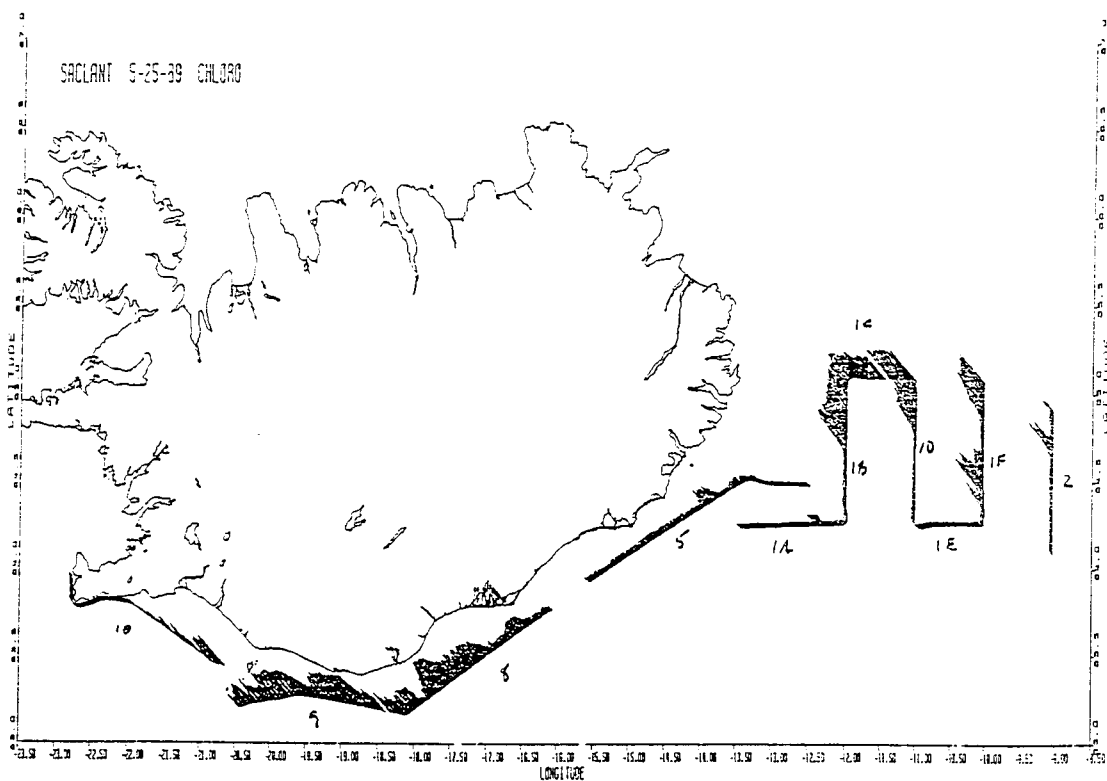
Fig. 9. Locations of AOL and MARS data tracklines during the front and eddy mapping mission of the NASA P3, over the southern Iceland shelf and the Iceland-Faeroe Ridge, on 25 May 1989. The "stick plot" shown for each flight segment illustrates the AOL chlorophyll estimates, with the length of each stick being proportional to chlorophyll concentration. This figure was provided courtesy of Dr. Frank Hoge of NASA WFC.
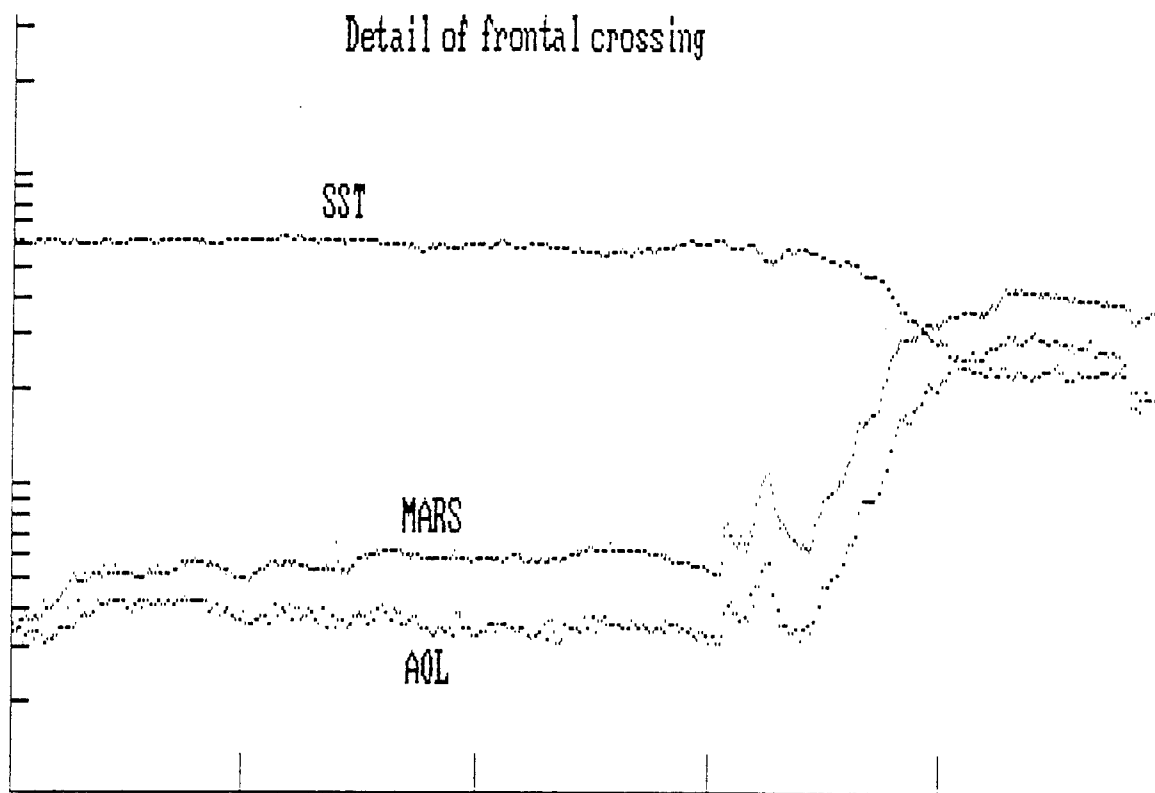
Detail of frontal crossing

SST

MARS

AOL

Fig. 10. Comparison of MARS and AOL chlorophyll estimates, together with the infrared sea surface temperature trace, extending from south (left) to north (right) along trackline 1D (Fig. 9) on 25 May 1989. The MARS and AOL chlorophyll traces are offset to facilitate visual comparison.